JTTEE5 20:1292–1309
DOI: 10.1007/s11666-011-9686-1
1059-9630/$19.00 © ASM International

HVOF-Deposited WCCoCr as Replacement for Hard Cr in Landing Gear Actuators

A. Agüero, F. Camón, J. García de Blas, J.C. del Hoyo, R. Muelas, A. Santaballa, S. Ulargui, and P. Vallés

(Submitted August 10, 2010; in revised form May 6, 2011)

WCCoCr coatings deposited by HVOF can replace hard Cr on landing gear components. Powders with two different WC particle sizes (micro and nano-) and geometries have been employed to study the effects on the coating's properties. Moreover, coatings produced employing two sets of parameters resulting in high and low flame temperatures have been evaluated. Minor differences in microstructure and morphology were observed for the two powders employing the same spraying parameters, but the nano-sized powder exhibited a higher spraying efficiency. However, more significant microstructural changes result when the low- and high-energy spray parameters are used. Moreover, results of various tests which include adhesion, wear, salt fog corrosion resistance, liquid immersion, and axial fatigue strength, indicate that the coatings produced with high-energy flame are similar in behavior. On the other hand, the nanostructured low-energy flame coating exhibited a significantly lower salt fog corrosion resistance.

Keywords adhesion, coatings, fatigue, hard Cr replacement, HVOF, landing gear, liquid immersion, microstructure, morphology, particle size, salt fog corrosion, WCCoCr, wear resistance

1. Introduction

Owing to their excellent wear resistance, electrodeposited hard Cr coatings have been extensively used since many years for a wide variety of applications, including bushing pins, printing and corrugating rolls, ball valves, machine tools, fittings, hydraulic cylinders, rotating shafts, bearing journals, aircraft landing gear, pistons, undersea oilfield equipment, etc. (Ref 1). Astonishingly, although these coatings have been industrially employed since about 1937, there is archeological evidence of the use hard Cr coatings 2200 years ago. For instance, a sword discovered in Emperor Quin Xi Huang's mausoleum in Xi'an, China was found to have a 10-15-μm layer (Fig. 1). Hard Cr coatings have been critical, up to present, for aircrafts, automotive components, and ships, both civil and military. However, there are crucial environmental and health issues related to the presence of hexavalent Cr (CrVI) from chromic acid, used during the plating process. CrVI is known to be carcinogenic and to cause a wide array of medical problems (Ref 2). Moreover, the plating process produces gas bubbles, responsible of the dispersion of chromic acid tiny droplets into the air. In addition, CrVI-contaminated rinse water must also be properly cleaned and disposed of, respecting regulations that not only vary from country to country but also are becoming more and more stringent. These issues have driven the production prices, related to workers' protection and waste disposal, to very high levels. For instance, in the Unites States, OSHA established a permissible exposure limit (PEL) of 5 $\mu g/m^3$ in 2006 (Ref 3). If, as expected, this limit is further reduced, the cost associated with the measures required to reach the new PEL will be in excess of several millions of dollars per year. Furthermore, in the Netherlands and the UK, there is already a pending legislation to reduce the PEL to 1.5 and 0.5 $\mu g/m^3$, respectively.

Research for new coating solutions has been extensive, yielding several potential alternatives. Essentially, the alternative coatings to hard Cr must be wear resistant, and moreover, the mechanical properties of the alternative material-coated components, such as fatigue strength, must be the same or better than those of said components coated with hard Cr. In addition, the new coatings must be resistant to environmental corrosion and to the attack of fluids commonly used on aircrafts, which may spill and therefore enter in contact with the coated components, so that their surface is not modified with the consequent losses in performance. Presently, carbide-based cermet coatings have exhibited the best results, especially in manufacturing and maintenance operations on military and civil aircrafts for components such as landing gears, propellers and hydraulic actuators (Ref 4). Deposited by high velocity oxyfuel (HVOF) thermal spray, these coatings are dense and exhibit very high adhesive strength and microhardness. HVOF is widely used in thermal spray technology by which particles are heated and propelled at very high velocities (>1 mach) resultant from the internal combustion of oxygen and fuel (propylene, kerosene, natural gas, hydrogen, etc.) and from the spray gun special

A. Agüero, F. Camón, J. García de Blas, J.C. del Hoyo, R. Muelas, A. Santaballa, S. Ulargui, and **P. Vallés**, Instituto Nacional de Técnica Aeroespacial, Ctra. Ajalvir Km 4, 28850 Torrejón de Ardoz, Madrid, Spain. Contact e-mails: agueroba@inta.es and modsurf3@inta.es.

Fig. 1 2200-year-old sword coated with 10-15 μm of Cr found in Emperor Quin Xi Huang's mausoleum in Xi'an, China

design. In particular, WCCoCr deposited by HVOF has been chosen as one the best candidates for landing gear components and a large number of groups worldwide have been studying it and testing this material for diverse applications (Ref 5-10). It exhibits, in most situations, a superior wear performance than electrolytic hard Cr, similar or according to some authors, better corrosion resistance (Ref 8, 11), and it does not affect the fatigue strength of the material. The coating is composed of WC particles in a matrix of Co with some Cr, and it also exhibits large features (5-10 μm) very rich in Cr. Cr is added to increase the atmospheric corrosion resistance.

However, there are several types of powders of this material available in the market, which exhibit different coating efficiencies (during spraying) and also resulting in different coating microstructures. One important characteristic of the powder is the WC particle size and is known, for instance, that if nano-sized WC particles are employed, the corresponding coatings exhibit higher hardness and wear resistance (Ref 12-15). The HVOF spraying parameters are as well crucial in determining the quality of the deposits and also influence the temperature reached by the component when it is being sprayed. This is critical especiallyfor landing gear actuators made of high strength steels (4340, for instance) which are shot peened to increase their fatigue strength, as its effect is lost if the component reaches temperatures higher that 177 °C (Ref 16). Moreover, the powder particles geometry may also affect both the resulting coating microstructure as well as the process as, for instance, it has been shown that spherical particles have better flowability (Ref 17).

WCCoCr coatings, produced from two different commercial powders with different powder grain geometries as well as WC particle size within each grain, have been deposited on 4340 low-alloy steel. The coatings, as well as a commercial electrolytic hard Cr coating, have been characterized and tested. Moreover, the influence of the coatings parameters on the coating microstructure and behavior have been studied employing two different sets of parameters resulting in high- and low-energy flames. Extensive characterization, as well as a number of tests were carried out to determine the influence of the microstructure and deposition parameters in the coating behavior, as well as to validate their performance as replacements for hard Cr on landing gear actuators. Characterization includes determination of microhardness, porosity, residual stresses, microstructure and phase composition of the coatings, and a comparison of the spraying efficiency obtained from both powders, whereas testing comprises adhesion, salt fog corrosion resistance, stability in liquids commonly employed on and around aircrafts, wear resistance, and axial fatigue strength. An industrially produced electrolytic hard chromium coating and 4340 steel as base material, was also tested as reference.

2. Experimental Section

2.1 Materials

Low-alloy steel 4340 (0.41C-0.73Mn-0.8Cr-1.74Ni-0.25Mo-0.25Si, wt.%) was obtained from Corus, United Kingdom. Specimens with geometries appropriate for each of the tests were machined and heat treated by GUTMAR, Spain. The ultimate tensile strength (σ_{us}) was 1200 MPa. Electrolytic hard chromium was deposited by CESA (Spain) according to standard QQC320 or MILSTD1501. WCCoCr powders Sulzer 5847 and Woka 3653 (A and B respectively) were obtained from Sulzer Metco Europe GmbH.

2.2 Coating Deposition

WCCoCr coatings were deposited employing a Sulzer Metco Diamond Jet Hybrid HVOF unit (A-3120) mounted on a six-axis robot (ABB) and fed by a twin rotation powder feeder. The spraying parameters for the three different studied coatings are shown in Table 1. Before coating, the specimens were grit blasted. Temperature measurement during coating was carried out by means of a calibrated Minolta/Land Cyclops 300AF infrared thermometer placed inside the deposition booth at a distance of approximately 750 mm from the component. The temperature was measured directly on the surface of the specimens, which were placed on appropriate sample holders. Particle velocity and temperature during spraying was measured by spray plume monitoring with Accuraspray-g3 (Sulzer Metco).

2.3 Microstructure and Composition

The microstructure and composition of the coatings was determined employing a scanning electron microscope (SEM) JEOL JSM 840 equipped with an energy dispersive X-ray spectrometer (EDS) KEVEX MICROANALYST 8000 which uses a signal processor RÖNTEC.

The porosity of the coatings as well as the phase composition was determined employing the LEICA Q550 MW image analysis program.

Table 1 HVOF spray parameters

	Oxygen, l/min	Hydrogen, l/min	Nitrogen, l/min	Powder feeder rate, g/min	Spray distance, mm	Transverse speed, mm/s
Coating A	214	344	635	38	230	1256
Coating B	214	344	635	38	230	1256
Coating B′	214	600	360	38	230	1256

Table 2 Rating criteria for the SALT FOG corrosion test

Range	10	9	8	7	6	5	4	3	2	1	0
Defects area, %	0	0-0.1	0.1-0.25	0.25-0.5	0.5-1	1-2.5	2.5-5	5-10	10-25	25-50	>50

The chemical composition of the powders was determined by a combination of two methods. Carbon was determined by combustion employing a LECO CS-444 analyzer. The rest of the elements were measured by X-ray fluorescence spectrometry employing a PHILIPS FRX PW2404 equipment. Quantification was carried out employing the semiquantitative IQ + He WIN method developed by PHILIPS to which the previously obtained carbon content was added.

X-ray diffraction (XRD) was carried out in a Panalytical X'Pert PRO MRD equipment with Cu K_α radiation at 45 KV and 40 mA. The scanning speed and scanning step were 2.4°/min and 0.02°, respectively. Quantification by means of the Rietveld method (Ref 18) was carried out employing the X'PERT HIGHSCORE PLUS software which includes a database.

The composition of the coatings as a function of depth was determined by glow discharge spectrometry (GDS) by means of a LECO GDS 850A equipment employing 30 mA and 800 V.

2.4 Residual Stress

The coatings were evaluated by preparing and spraying a standard Almen Type ''N'' specimen strip with identical parameters as the coating being evaluated. The Almen test is employed to determine shot peening intensities by measuring the curvature caused by peening on a standardized flat coupon. This measure is related to the stresses generated on the coupon by the process and can also be used to evaluate the relative residual stresses imparted to the substrate-coating system during thermal spraying (Ref 16). The curvature of the Almen strip was less than 0.051 mm (arc height) when measured before coating. After coating, measurements were carried out with the convex surface facing up and employing a standard Almen gage (AMS S13165). During coating, the strip was restrained in a flat position by four screws as indicated in AMS S13165. The reported normalized value was obtained from the difference between the measures taken from the coated and uncoated strips, according to AMS 2447.

2.5 Hardness Measurements

Vickers microhardnesses were measured according to ASTM E 384 using a Future Tech FM system, from 10 evenly spaced indentations on the cross section of the coatings (minimum thickness of 200 μm), employing a 300 g load.

2.6 Adhesion Measurement

2.6.1 Bend Testing. Bend testing was carried out according to AMS 2447 using three specimens (100 × 50 × 2 mm) coated on one side. The specimens were bent 90° around a 8-mm Ø mandrel with the coated side on the outside of the bend, and examined visually. If cracks appeared, attempts were made to remove the coating by means of a sharp blade. Cracking or peeling near the edges was not considered or taken into account when evaluating the bent specimen.

2.6.2 Bond Strength Measurement. The bond strength measurement was carried out according to ASTM C 633, ''Adhesion or cohesion strength of thermal spray coatings.'' The test was performed on a Universal Test Machine by constantly increasing the tensile load at 0.017 mm/s employing HTK Ultrabond 100 as adhesive. The hard Cr-coated samples were machined to 0.4 μm Ra, while WCCoCr was tested as deposited.

2.7 Salt Fog Corrosion Testing

The salt fog corrosion testing was carried out according to ASTM-B-117. Five 150 × 75 mm specimens per coating are exposed to a mist generated from a 5 wt.% NaCl aqueous solution (pH within 6.5-7.2) at 35 °C for a total of 1056 h. Before coating the specimens, edges and backside were masked with a suitable corrosion-protective paint. The coupons were visually inspected and assigned a protection rating according to ASTM-B-537-70 (see Table 2) every 24 h. The rating reported for each condition is the average of those obtained for the five tested specimens. If the rating was lower than 3, the specimen was mechanically cleaned by means of a ''Scotch Brite''-type pad to eliminate corrosion products, and the samples were rated again.

2.8 Liquid Immersion Resistance

Three coated coupons (25.4 × 25.4 × 0.8 mm) were totally immersed on each of the liquids and temperatures indicated in Table 3. The liquids were chosen among the most currently employed in aircrafts. The samples were held vertically and were inspected and weighted every 24 h, removing the liquid by means of a solvent appropriate for the corresponding liquid for a total of 168 h. At

Table 3 Fluids and temperatures employed for the immersion test

Fluid	Type	Temperature (±2 °C)
MIL-L-23699	Oil lubricant	70
JP-8	Fuel	70
Skydrol LD4	Hydraulic	70
MIL-PRF-87257	Hydraulic	70
PD-680 Type II	Degreaser	23
Propylene glycol/water 1:3 (V)	Antifreeze	23

Table 4 Rating criteria for the liquid immersion test

0	Without detectable bleaching or corrosion
1	Light corrosion and/or bleaching up to 5% of the surface
2	Light corrosion and/or bleaching up to 10% of the surface
3	Light corrosion and/or bleaching up to 25% of the surface
4	Light corrosion and/or bleaching up to 25% of the surface and/or presence of pits

each inspection, a protection rating is attributed as shown in Table 4.

2.9 Wear Test

Wear testing was carried out by means of a ball-on-disk tribometer (CSEM). The test conditions were the following: applied load, 10 N; sliding distance, 1000 m; sliding speed, 10 cm/s; temperature, (23 ± 2) °C; and relative humidity, (35 ± 5)%. Alumina balls (6.35 mm Ø) with surface roughnesses within the range 0.07-0.1 μm Ra and hardness ranging between 1650 and 1800 HV were employed. The coated specimens were finished to 0.1-0.2 μm Ra. The wear test results were calculated by a Taylor Hobson Form Talysurf Profilometer.

2.10 Axial Fatigue Strength

For the axial fatigue strength test, a sinusoidal load of 20 Hz with load ratio of $R = -1$, at room temperature (23 ± 2 °C) and 35 ± 3% humidity was applied throughout this study. Experimental tests consider as fatigue strength the specimen fracture or 5×10^6 load cycles. The test was performed on two MTS computer-controlled servohydraulic axial fatigue testing machines, according to the ASTM E466 standard.

The samples were not shot peened before coating and/or testing. Three groups of fatigue specimens were prepared to obtain S-N curves:

- 24 specimens of 4340;
- 12 specimens of 4340 hard Cr coated;
- 24 specimens of WCCoCr (coating B) coated 4340.

Four stress levels were chosen for the tests:

- 670 MPa (56%σ_{us}), 620 MPa (52%σ_{us}), 570 MPa (47%σ_{us}), and 520 MPa (43%σ_{us}), for hard Cr and WCCoCr samples;
- 790 MPa (66%σ_{us}), 750 MPa (63%σ_{us}), 710 MPa (59%σ_{us}), and 670 MPa (56%σ_{us}), for uncoated 4340;

The average surface roughnesses (R_a) of specimens were

- Specimens of base material (40 HRC): $R_a = 0.65$ μm;
- Specimens coated with hard Cr: $R_a = 0.90$ μm;
- Specimens with B coating: $R_a = 4.30$ μm (as sprayed)

All surface roughness data were obtained using a Taylor Hobson Form Talysurf Profilometer using a 0.8 mm cut-off.

The fatigue experimental program was performed on round specimens with continuous radius between ends, machined according to Fig. 2. The stress was determined taking into consideration the coating thickness.

3. Results

3.1 Powder Characterization

Figure 3 shows the microstructure of the two starting powders, whereas Table 5 includes the corresponding compositions (in wt.%). Agglomerated and sintered, powder A (Sulzer 5847) has a grain size distribution of −53 + 11 μm. It is composed of irregular spheres with lower W and higher Cr and Co contents and a significantly WC higher particle size than powder B, oscillating between 2 and 8 μm (the largest particle dimension). It also exhibits the Cr-rich features mentioned earlier, typical of this commercial powder. Powder B (Woka 3653) also agglomerated and sintered is spheroidal in shape with a grain size distribution of −45 + 11 μm. In this case, the WC particles size fall between 100 nm and 3 μm. XRD also indicated differences in the composition of the two powders as shown in Fig. 4 and Table 6 where the diffraction patterns and the phase composition (according to the Rietveld method) are respectively included. Both powders exhibit peaks corresponding mostly to WC with very small peaks that can be assigned to W, Co, and η phases W_3Co_3C or W_6Co_6C. The peaks attributed to either of those two phases are slightly shifted likely because of the presence of Cr in the lattice. According to Berger et al., the η phase peaks are attributed to W_3Co_3C (Ref 19) whereas other authors, for instance, Verdon et al. attribute them to W_6Co_6C (Ref 20). According to the Rietveld analysis, powder A appears to have more crystalline matrix phases, whereas powder B is richer in the carbide phases. The η phases could not be quantified by this method because the corresponding diffraction patterns have not been included in the database employed for the analysis.

3.2 Deposition Process

One of the main difficulties related to HVOF coating deposition on landing gear components is the heat transfer from the flame to the components, which as already

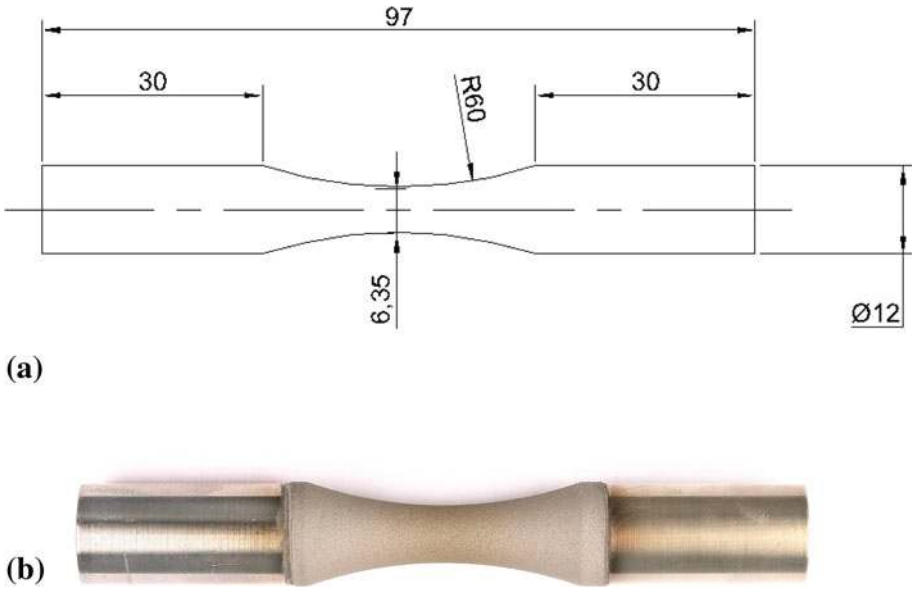

Fig. 2 Fatigue specimens. All the dimensions are in mm. (a) Drawing and (b) as WCCoCr sprayed

mentioned, need to be shot peened before coating to increase their fatigue strength, especiallywhen coated with electrolytic hard Cr (Ref 16). If the component surface reaches temperatures higher than a critical value (177 °C for 4340 steel), the effects of the shot peening treatment in increasing the fatigue strength are lost. As a general rule, in order to produce dense coatings without unmelted particles, spraying parameters resulting in high flame temperatures are required, but if these parameters are used, the component will reach high temperatures, and therefore will require external cooling by means of CO_2 or liquid N_2. Coatings A and B were deposited from the corresponding powders, following the procedure recommended by SAE AMS2447-9 and employing the same set of spraying parameters based on the powder manufacturer recommendations (Table 1). The coatings were optimized to (a) reduce porosity to offer adequate protection from environmental corrosion; (b) reduce residual stresses to prevent crack development and coating delamination; (c) keep the hardness between 900 and 1100 HV as, if the coating is not hard enough, the wear resistance would not meet requirements, whereas if it is too hard, the required finishing process will be too difficult and finally; and (d) maximize the powder spray efficiency to reduce cost. However, using small variations of all parameters did not result in significant improvements relative to the parameters recommended by the powders' manufacturers. These parameters produce a high-temperature flame requiring external cooling of the component with liquid N_2 during spraying, to keep the component surface below 177 °C. As cooling increases the processing costs, attempts to reduce the flame temperature were carried with powder B which exhibited the best spraying efficiency when employing the manufacturer's parameters (Table 7). The flame energy was therefore reduced to keep the component surface temperature to a minimum value, and at the same time, maximize the spraying efficiency and optimize the coating quality (coating B′).

During spraying, the samples' temperatures were measured by means of an IR thermometer, and continuous, real-time, online monitoring of in-flight particle velocities and temperature was carried out to ensure control and stability of the system spray parameters by means of the Accuraspray online monitoring device. Table 7 shows the Accuraspray data as well as spraying efficiencies for coatings A, B, and B′. The obtained temperatures and velocities are employed only for comparison purposes. The particle velocity resulting from powder A was lower than that obtained from powder B. This is certainly due to the reduction in WC particle size as observed by Bouaricha and Legoux (Ref 21) as well as to the slightly smaller grain size. Moreover, the temperature of the particles in the flame obtained when using powder B was slightly lower than that produced using A. According to Li et al.'s results based on multi-scale modeling of the HVOF process for WCCo (Ref 22), the particle velocity and the particle melting degree strongly influence the coating microstructure. Those authors have also shown that the higher the particle density, the lower is the temperature reached by the particle during spraying. This is the case with powder B due to smaller WC particle size, as there are more, heavier particles of WC in each agglomerated grain that is being sprayed (Fig. 3). The parameters chosen for B′ resulted in a significantly lower particle temperature, as expected when reducing the flame energy. Coatings A and B required abundant cooling with liquid N_2 during spraying, whereas for B′ cooling with air was sufficient.

Finally, there were important differences in the spraying efficiency obtained from the two powders: powder A, with higher WC particle size and irregular spherical particles, resulted in a spraying efficiency significantly lower. As a result of a study carried out for Cr_3C_2-NiCr (Ref 23),

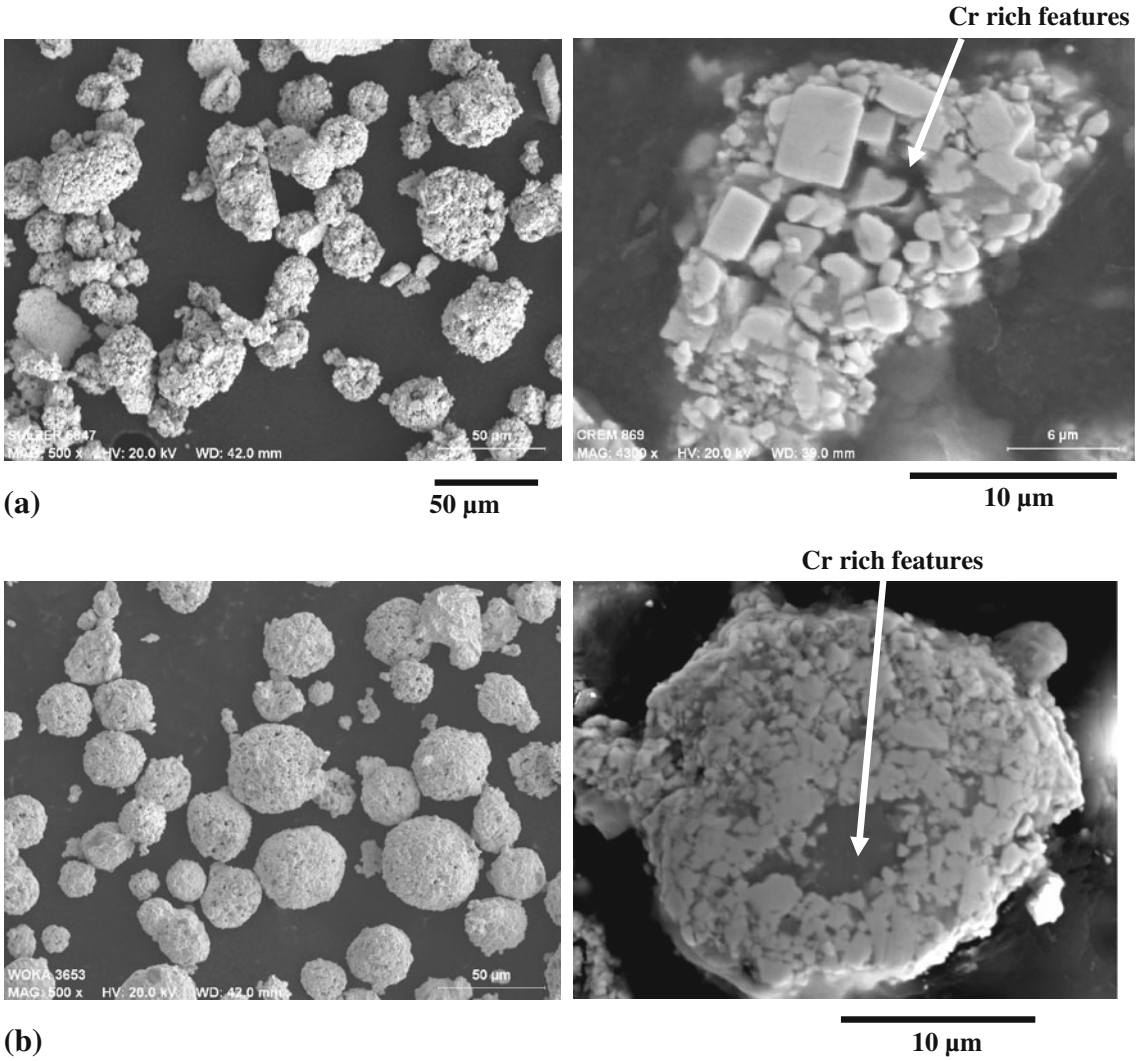

Fig. 3 WCCoCr powders: (a) powder A and (b) powder B

Table 5 WCCoCr powder composition

	W	C	Fe	Co	Cr	Ni
A	80.16	5.50	0.30	8.80	5.20	0.04
B	83.19	5.20	0.20	7.7	3.70	0.01

Li et al. concluded that carbide rebounding during spraying increases with carbide particle size and therefore, the larger the carbide particle size, the higher is the amount of wasted powder. Moreover, as already mentioned, the flowability of spherical powders such as powder B is higher.

3.3 Coating Characterization

The microstructures of the coatings A, B, and B′ are shown in Fig. 5(a)-(c), respectively; moreover, image analysis was carried out to determine the degree of porosity as well as to obtain the coatings phase composition, and the corresponding results are presented in Fig. 6(a)-(c) and Table 8. Four different microstructural features could be observed in the micrographs of the three coatings: (a) WC as light particles with angular edges and therefore unmelted during spraying (yellow in Fig. 6); (b) a gray zone corresponding to the matrix, not only rich in Co but also containing Cr, W, and C (green in Fig. 6); (c) dark large ''agglomerates'' also within the matrix, rich in Cr but with some C (red in Fig. 6); and finally (d) black pores (blue in Fig. 6). Although decarburization of WC will likely result in formation of CO and/or CO_2, the amount of C detected by EDS was considered to be significant. Porosity was very low for the three coatings, but lower for both coatings B and B′ obtained from the smaller WC particle powder. The relative content in WC follows the trend A < B < B′, whereas that of the Cr-rich agglomerates is quite the opposite.

In Fig. 7, the microstructure of the electrolytic hard chromium coating employed as a reference, is shown for comparison purposes. A pattern of fine cracks (in some cases, through-thickness) can be observed, and the porosity degree is of 0.6%.

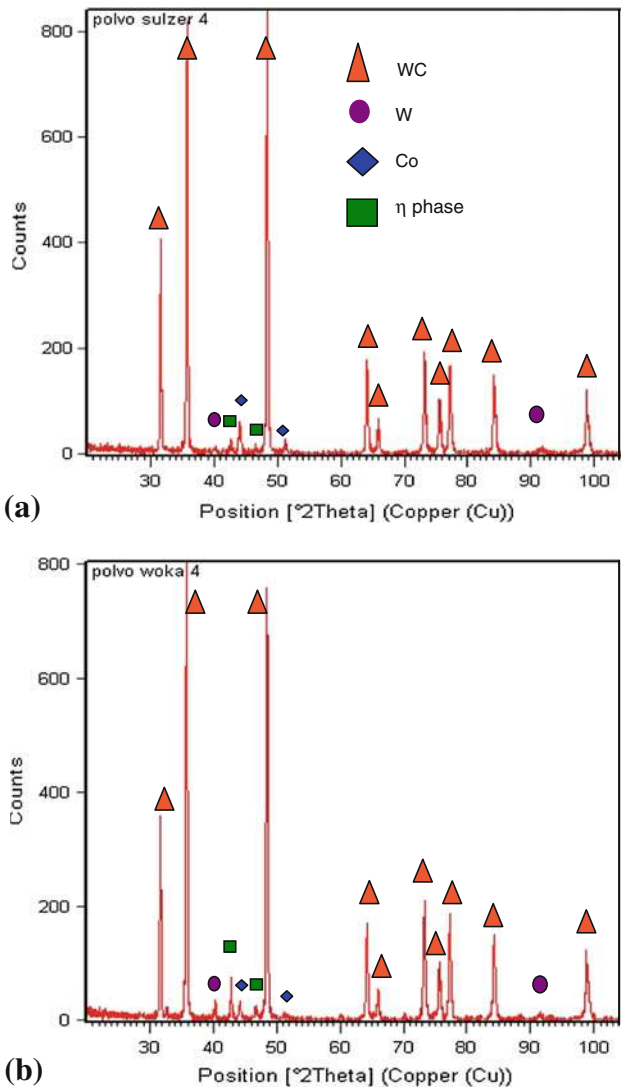

Fig. 4 XRD patterns of the WCCoCr powders: (a) powder A and (b) powder B

Table 6 Phase content of the WCCoCr powders determined by XRD (Rietveld method)

	WC, wt.%	W, wt.%	Co
Powder A	88.5	0.5	11.0
Powder B	93.1	2.7	4.2

Depth profiling of the coatings was carried by GDS (Fig. 8a-c), and the corresponding elemental composition measured at half the thickness as depth is shown in Table 9. Coating A exhibits a slight variation in composition as a function of thickness (Fig. 8a) and significantly higher oxygen content than the other two coatings. This higher oxidation degree may be caused by the slightly higher particle temperature observed during spraying, as in particular, with the lower particle velocity resulting in the particles spending more time in the flame and therefore having more time to oxidize. Moreover, in coating B′, the total carbon content appears higher than in the other two layers, probably as a result of less decarburization due to the lower flame temperature. The compositions of all coatings have significantly changed relative to the corresponding powders, with less W possibly indicating important losses during deposition by WC particle rebounding (analysis by EDS confirmed these results).

XRD of coatings A and B (Fig. 9) exhibited broadened peaks attributed to WC, W_2C, and W as well as a broad peak at $2\theta = 43°$ indicating the formation of an amorphous phase in agreement with other groups (Ref 24-27), but at different relative intensities. Li et al. (Ref 24) found that when heating a HVOF-sprayed WCCo coating to 600 °C, this peak disappeared, whereas new peaks corresponding to Co_6W_6C, Co, graphite, and W appeared. In contrast, coating B′ only had peaks corresponding to WC, W, and η-phase (as mentioned before, it was not possible to distinguish between Co_3W_3C and Co_6W_6C), whereas the 43° peak was absent. These results indicate that the high temperatures at which the particles are subjected when high-energy flame conditions are employed, as for coatings A and B, may be responsible for the loss of crystallinity of the material during spraying and also for the decomposition of the η-phase. The phase composition was also determined by the Rietveld method as shown in Table 10. Coatings A and B exhibited relatively higher amounts of W_2C and a consequent a decrease in the WC content relative to the corresponding starting powder, certainly as a result of decarburization during spraying in agreement with the results of Verdon et al. when spraying WCCo (Ref 20). The variation in the degree of decarburization observed for the two coatings, measured by the difference between the WC present in the starting powder relative to that in the coating, was small and may be attributed to the slightly different observed particle temperatures during spraying: as in coating B which exhibited a lower flame temperature (Table 7) than coating A, slightly less WC has decarburized. These results are also in agreement with those obtained by Chivavibul et al.

Table 7 Flame parameters measured with Accuraspray-g3 (measured at the spraying distance) and spraying efficiency

	Powder grain size, μm	Velocity, m/s	Temperature, °C	Spraying efficiency (a), μm/g
Coating A	−53 + 11	520	1870	1.98
Coating B	−45 + 11	600	1820	2.97
Coating B′	−45 + 11	584	1310	4.74

(a) The spraying efficiency was calculated on the basis of microns of deposited coating per gram of powder

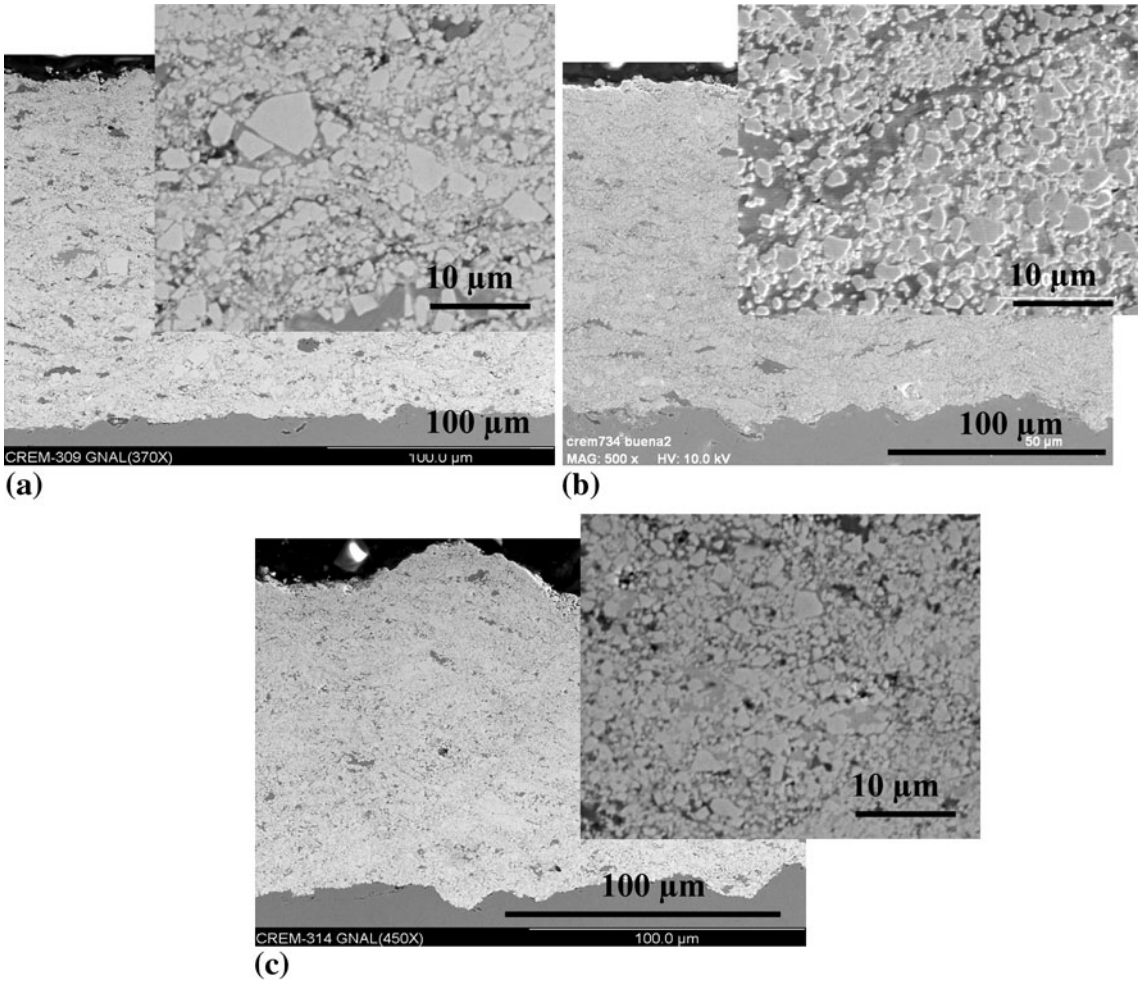

Fig. 5 SEM cross-sectional images of WCCoCr coatings deposited by HVOF: (a) coating A obtained from powder A with a high-energy flame, (b) coating B obtained from powder B with a high-energy flame, and (c) coating B′ obtained from powder B with a low-energy flame

(Ref 26) who found a correlation between particle size and decarburization; the larger the particle size, the higher the decarburization—in this case based on the total amount of C present in the coatings. However, other authors, for instance, Berget et al. (Ref 27) and Guilemany et al. (Ref 15), have found quite the opposite trend attributing their results to overheating of the smaller particle size and therefore increasing the chemical reactivity. In addition, Guilemany concluded that higher decarburization is observed for lower particle sizes because of the higher surface contact area of these particles as a result of higher surface to volume ratio. As seen in Table 7, the variation in the particle temperatures observed when spraying coatings A and B is quite low and perhaps the magnitude of the differences (<10%) in the measured WC content may not be very significant.

The W_2C phase could not be observed in the micrographs as already mentioned. Chivavibul et al. pointed out (Ref 26) the particles may be very fine and dispersed in the matrix but Stewart et al. (Ref 28) and Verdon et al. (Ref 20) employed transmission electron microscopy to observe this phase as a shell around the WC particles on WCCo coatings. As mentioned earlier, the Co-rich gray phase observed by SEM also contains significant amounts of W and C, and is moreover, it is present in higher proportion in coating A in agreement with a larger decarburization degree. In addition, in coating B′, deposited with a significantly lower particle temperature, the amount of W_2C was too low to be measurable.

The image analysis compositions may not be compared with the Rietveld results (Table 8 and 10, respectively) as in the first case some of the crystalline phases observed by XRD such as W_2C cannot be observed, as already mentioned, and conversely in XRD, non-crystalline phases such as the matrix are absent. It is interesting, however, to note that. in both cases. the WC content follows the same tendency: A < B < B′, and moreover, that the coatings A and B produced with high-energy flame, have a significantly lower WC content than the original powders A and B.

The three studied coatings exhibited relatively low compressive residual stress evaluated by Almen strip deflection (the curvature caused by coating deposition) as

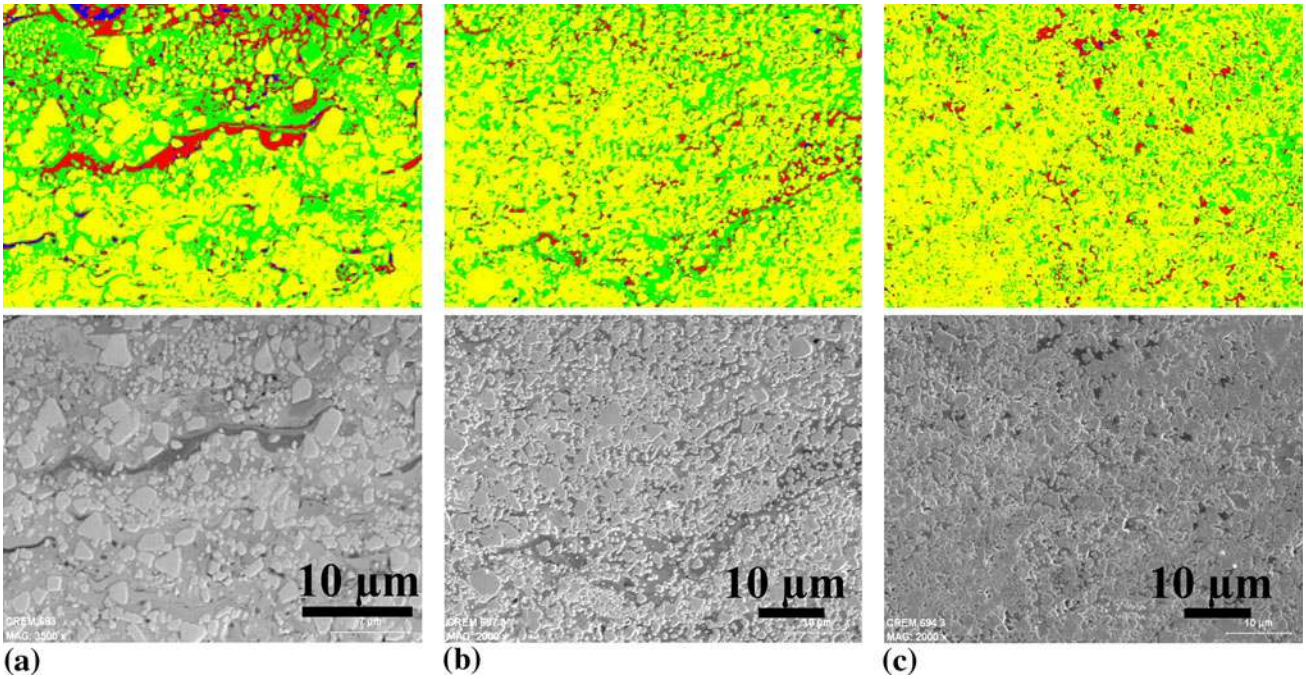

Fig. 6 Samples employed to carry out phase image analysis of WCCoCr coatings deposited by HVOF: (a) coating A obtained from powder A with a high energy flame, (b) coating B obtained from powder B with a high energy flame and (c) coating B′ obtained from powder B with a low energy flame (WC: light gray, Co with some Cr, W and C: medium gray, Cr with some C: dark gray and pores: black)

Table 8 Phase content of the WCCoCr coatings determined by image analysis

	WC	WCCoCr	CCr	Porosity
Coating A	50.4	40.7	8.4	0.5
Coating B	59.6	35.1	5.3	0.1
Coating B′	74.3	22.3	3.3	0.1

shown on Table 11 (Almen values within the +0.076 to −0.305 mm range are considered acceptable for this application (Ref 29): the higher the deflection, the higher is the compressive stress). Moreover, there is a correlation between the particle temperature and the stress for the three coatings with coating A, exhibiting both the highest temperature during spraying and the highest compressive stress, in agreement with Legoux and Bouaricha (Ref 29) as well as Ibrahim and Berndt (Ref 30), who have indicated that the residual stress that develops in a thermal-spray-coated surface is mostly related to the thermal conditions to which the coating-substrate system has been subjected, as a result of quenching stresses that arise during deposition and cooling during post-deposition. Moreover, it has been shown that the fatigue strength of the coated components can be increased by introducing compressive stresses into the surface (Ref 31); however, these stresses must not be too high or else the coating will spall during cooling.

The Vickers microhardness of coatings A, B, and B′ as well as that of the electrolytic hard Cr coating are shown on Table 12. The three WCCoCr coatings were harder

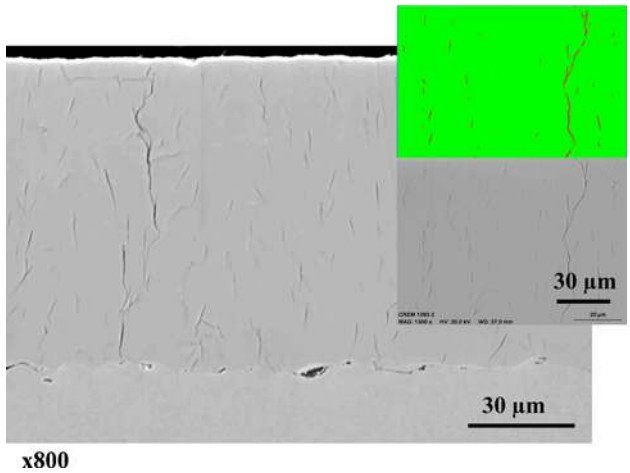

Fig. 7 SEM cross-sectional images including a sample employed for the phase image analysis of electrolytic hard chromium

than the Cr reference. On the other hand, the hardness of coating B′ is significantly lower than that of the other two coatings due to the lower flame energy parameters employed during its deposition. These results are in agreement with Zhao et al. (Ref 32) who observed the same trend. The results are also in agreement with the high content of W_2C present in coatings A and B, as W_2C is significantly harder (H_V: 3000) than WC (HV: 1300-2300) (Ref 33), whereas as already mentioned, in the softer coating B′, there is no W_2C according to the XRD

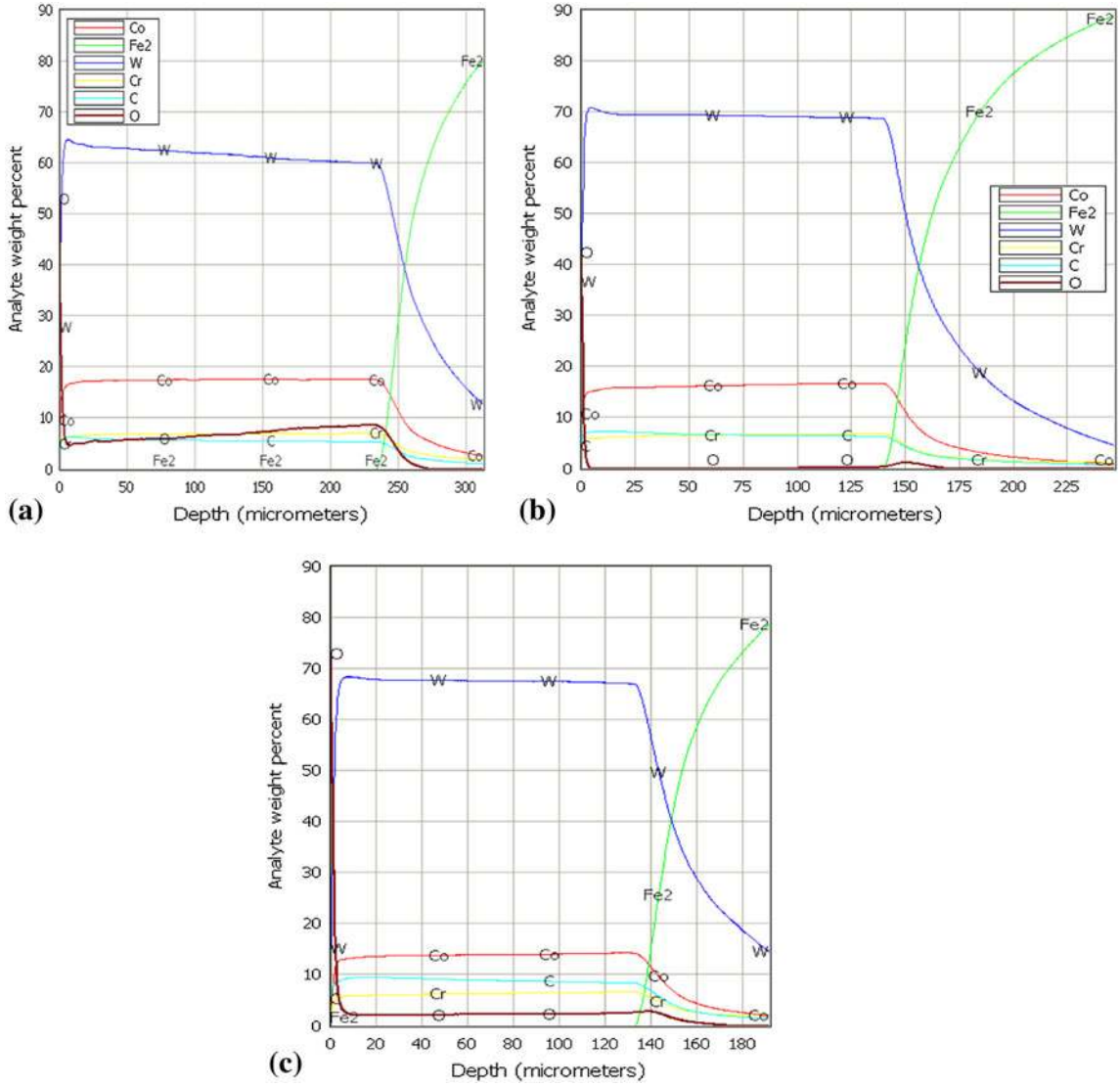

Fig. 8 GDS depth profiling of the three WCCoCr coatings: (a) coating A, (b) coating B, and (c) coating B′

Table 9 Elemental analysis of the WCCoCr coatings determined by GDS (wt.%)

	W	Co	Cr	C	O
Coating A	64.22	18.05	7.18	4.63	4.07
Coating B	69.20	16.26	6.54	6.56	0.00
Coating B′	67.50	13.88	6.28	8.87	2.17

analysis. Bouaricha and Legoux (Ref 21) observed an opposite trend, i.e., the higher the decarburization, the lower the hardness, but their decarburized coating showed very high amounts of W (38-47 wt.%) which is certainly significantly softer (HV: 349) (Ref 34) than the two carbides. A and B exhibit the same hardness values despite the difference in WC particle size and also in W_2C content. However, the magnitude of this last difference may not be significant enough to have an effect in the coatings hardness, as already mentioned.

3.4 Adhesion

Coated specimens were bent to 90° around an 8-mm-Ø mandrel, and no evidence of coating delamination could be observed in any of the samples. In Fig. 10, a bent specimen per each of the different WCCoCr coatings is shown including hard Cr for comparison purposes. Moreover, for the three WCCoCr coatings, the adhesion strength was higher than 89 MPa, as failure always occurred within the adhesive. For the hard Cr coating, failure occurred at the coating substrate interface at 100 MPa.

3.5 Salt Fog Corrosion

Uncoated specimens as well as two different deposition batches of electrolytic hard Cr-coated specimens (both with a coating thickness of ≈100 μm) were included to illustrate the lack of repeatability typical of this coating, as small variation on processing parameters have strong effects on the coatings quality. The thickness of each of

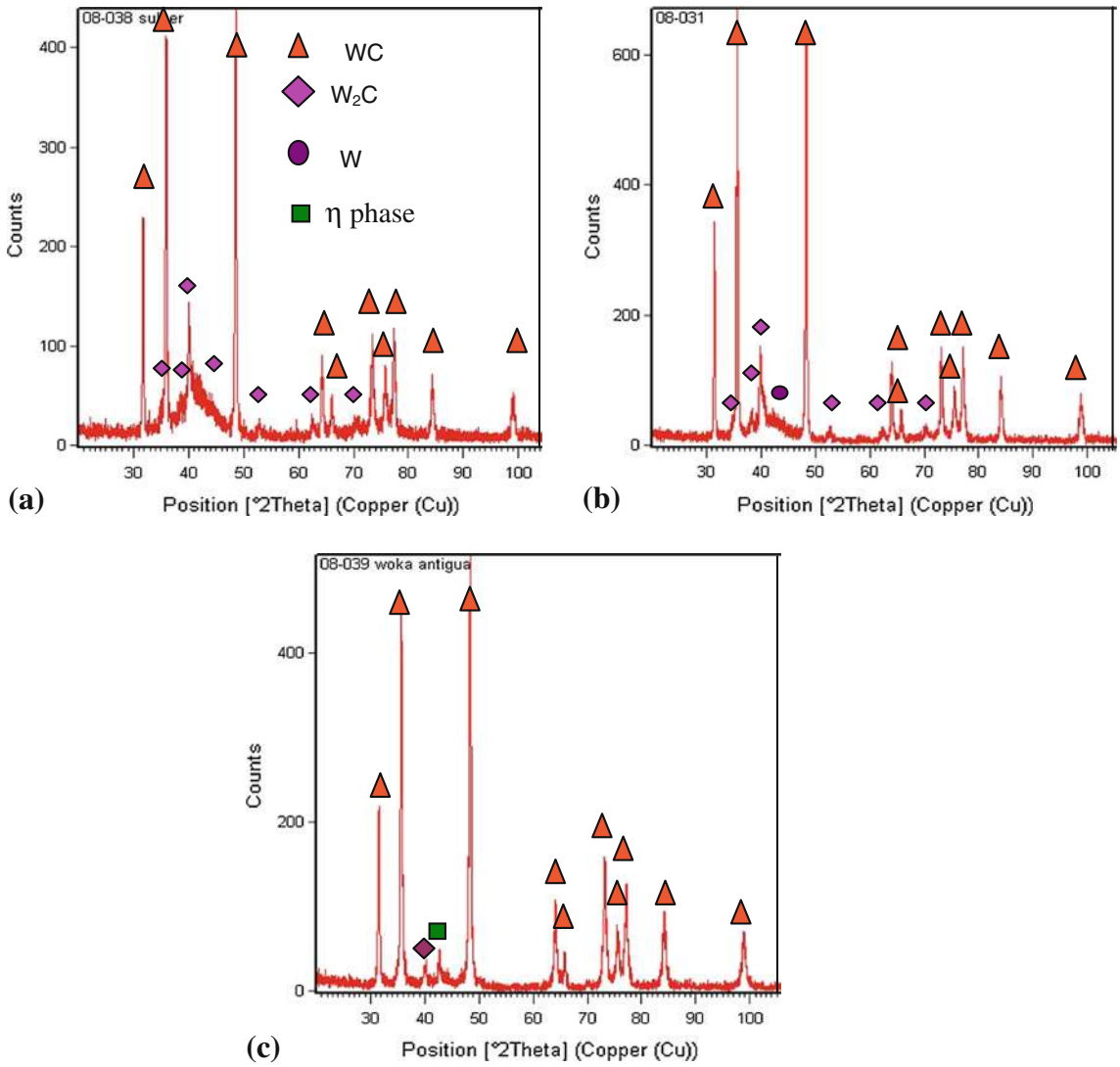

Fig. 9 XRD patterns of the three WCCoCr coatings: (a) coating A, (b) coating B, and (c) coating B′

Table 10 Phase content of the WCCoCr coatings determined by the XRD (Rietveld method)

	WC, wt.%	W_2C, wt.%	W, wt.%
Coating A	68.4	29.2	2.4
Coating B	76.8	20	3.2
Coating B′	97.0	…	3.0

Table 11 Almen strip deflection of the WCCoCr coatings

	Deflection, mm
Coating A	0.29
Coating B	0.15
Coating B′	0.11

the three WCCoCr coating was ≈150 μm, and exposure was carried out for a total of 1000 h. The progression of the ratings (after removal of the corrosion products) is represented on Fig. 11, whereas images of representative specimens after exposure and before removal of the corrosion products are shown in Fig. 12.

The uncoated specimens were totally covered with corrosion products after only 24 h as expected. Regarding the hard Cr-coated specimens, different results were obtained for each batch. From Fig. 11 and 12, it can be seen that the hard Cr coating obtained from batch 1 exhibited very poor corrosion resistance with a ranking of 4 after only 24 h caused by excessive, generalized blistering, leading to corrosion pits, whereas batch 2 exhibited better behavior with only localized blistering, mostly near the specimen edges and a ranking of 4 after 1000 h. Electrolytic hard Cr coatings exhibit a microcracked morphology which develops to relieve high residual stresses originating from the deposition process (Ref 35). Published data from other research groups also show

diverse results when salt fog testing the hard Cr coating. In some cases, the differences in behavior are associated to different coating thicknesses as several authors have indicated that the higher the thickness the better the corrosion resistance. It is not the case in the present investigation, as both batches exhibited the same coating thickness. Other groups have associated the differences in corrosion resistance to uncontrolled processing parameters during production resulting in different degrees of microcracking (Ref 5, 7, 8, 22, 25, 36).

On the other hand, WCCoCr coatings A and B exhibited excellent behavior and certainly, significantly better than that of the best hard Cr coating (resulting from batch 2). Both coatings exhibited a ranking of 7-8 after 1000 h of exposure, and there was a significant difference between them, as on coating A there was some degree of corrosion near the corresponding specimen edges. However, ASTM 117 indicates that corrosion near the edges must be disregarded. Dudzinski et al.'s results (Ref 8) on the same type of coatings on Aermet 100 and 300 M indicated that a thickness of 76 μm exhibited pitting already after 500 h, whereas those with 254 μm did not corrode, and the coated samples were only discolored after 1000 h. Bodger et al. employed 200-μm-thick WCCoCr and did not observe corrosion products after 30 days of exposure to the salt spray test (Ref 37). From the present results, it can be concluded that such high thicknesses are not required for the coatings to protect 4340 from salt fog corrosion. On the other hand, coating B′, sprayed with a low-energy flame to reduce heating of the component, showed a much lower resistance to salt fog corrosion exhibiting large blisters and a ranking of 2 after only 144 h of exposure. This observation suggests that corrosive agents could open a path to the substrate and corrode it. Most authors agree that corrosion occurs via path ways such as through-thickness cracks, interconnected porosity, interlamellar or unmelted particles boundaries, or micro-cracking (Ref 38-41). As already mentioned, this coating has very low porosity and at a similar level than that of coating B (0.1%) as seen in Fig. 6 and Table 8, but the resolution of the SEM may not be high enough to show very fine pores and cracks that allow the passage of H_2O/NaCl molecules all the way to the substrate (Ref 36). Figure 13 shows the cross section of corroded B′ after 144 h of salt fog spray exposure. It is observed that there is no evidence of either micro-cracking or porosityor unmelted particles or clearly defined

Table 12 Vickers microhardness of the coating

	Microhardness ($HV_{0.3}$)
Hard chrome	850
Coating A	1200
Coating B	1200
Coating B′	1000

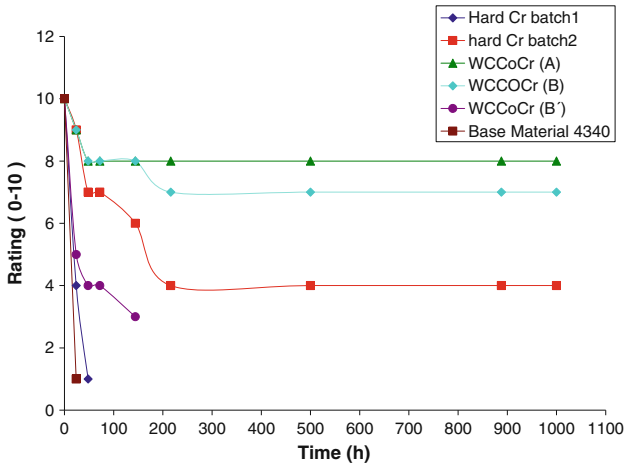

Fig. 11 Rating of the tested specimens when exposed to a salt fog corrosion atmosphere

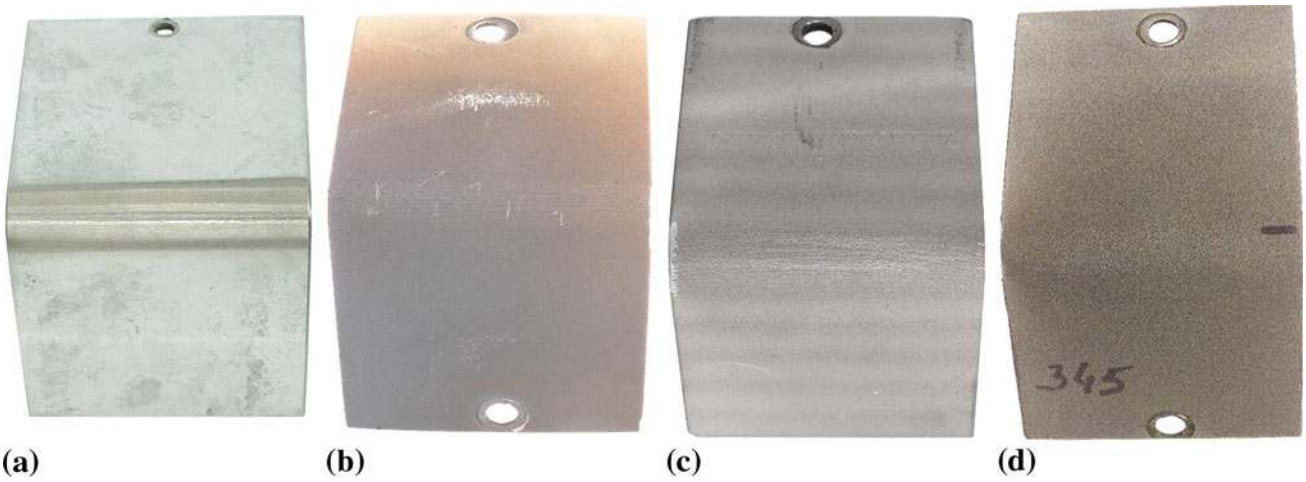

Fig. 10 Bend test results: (a) hard Cr, (b) WCCoCr (A), (c) WCCoCr (B), and (d) WCCoCr (B′)

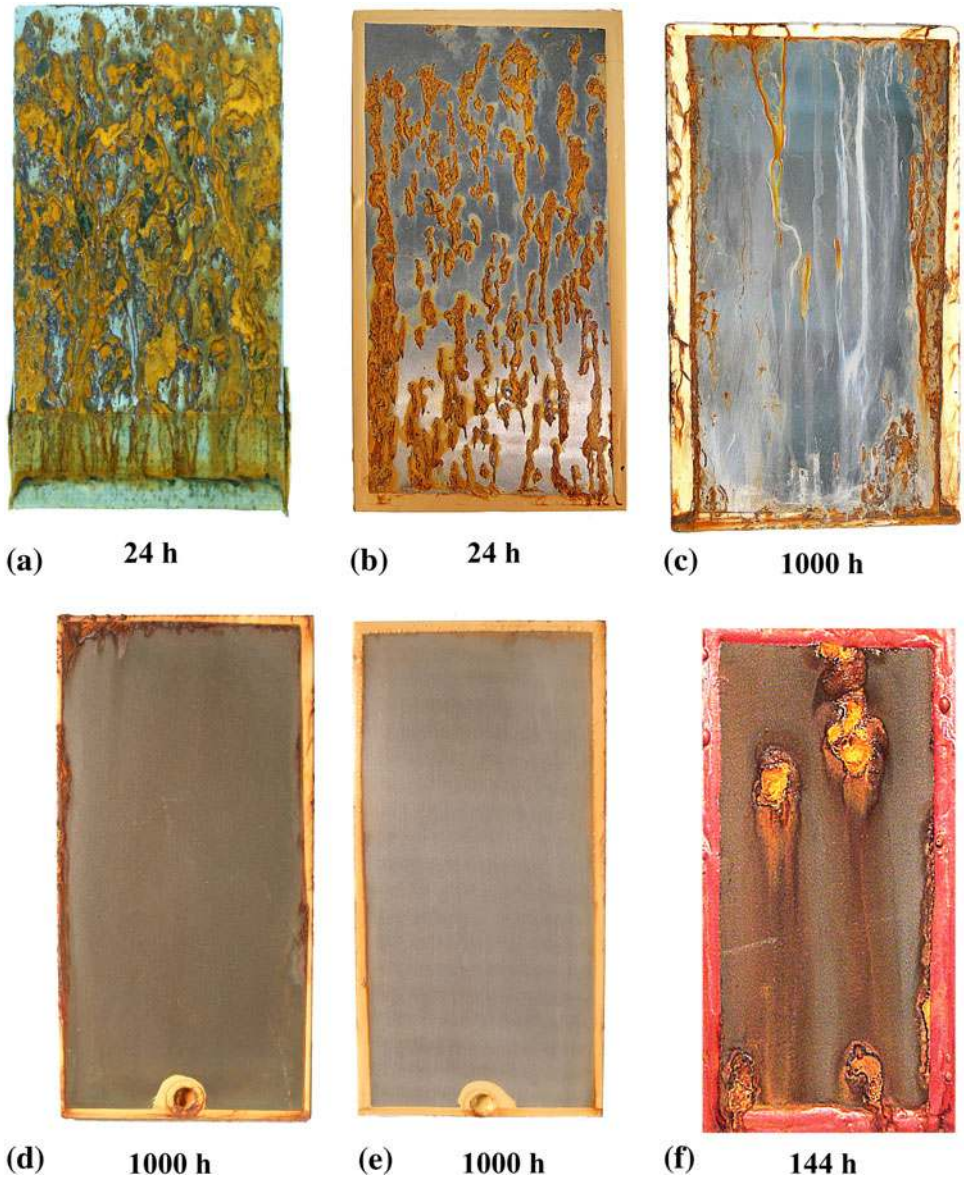

Fig. 12 Salt fog corrosion test results: (a) uncoated 4340 steel, (b) hard Cr (batch 1), (c) hard Cr (batch 2), (d) WCCoCr (A), (e) WCCoCr (B), and (f) WCCoCr (B′)

interlamellar boundaries. Nevertheless, the substrate corrosion products have permeated the coating (and are actually present within it), even reaching the coating surface. The corrosive attack may be associated to the lower matrix/particles volume ratio observed in coating B′, and therefore, to the lower Cr content, as Cr is mostly present in the matrix, or as carbide, but only that present in the matrix is available to contribute to increase the corrosion resistance. Moreover, corrosion may proceed through the relatively higher level of WC particle boundaries as there are significantly more such particles per coating volume in this layer, than in the other two coatings. It has actually been shown that Cr-free coatings, such as WCCo (Ref 5) and WCNi (Ref 42) coatings, are significantly less resistant to corrosion than WCCoCr. Moreover, Cr_3C_2NiCr is also more resistant to salt spray corrosion than WCNi (Ref 42). As mentioned before, corrosion may also proceed through interconnected porosity, too fine to be observed by SEM.

3.6 Liquid Immersion Testing

Aeronautic components are exposed to a wide variety of fluids currently employed for different purposes, such as fuels, antifreezes, hydraulic fluids, lubricants, degreasers, etc. Therefore coatings employed on said components must be resistant to these fluids. After immersion in the liquids indicated in Table 3 for a total of 168 h, all of the tested specimens had a rating of 0. Indeed, coatings

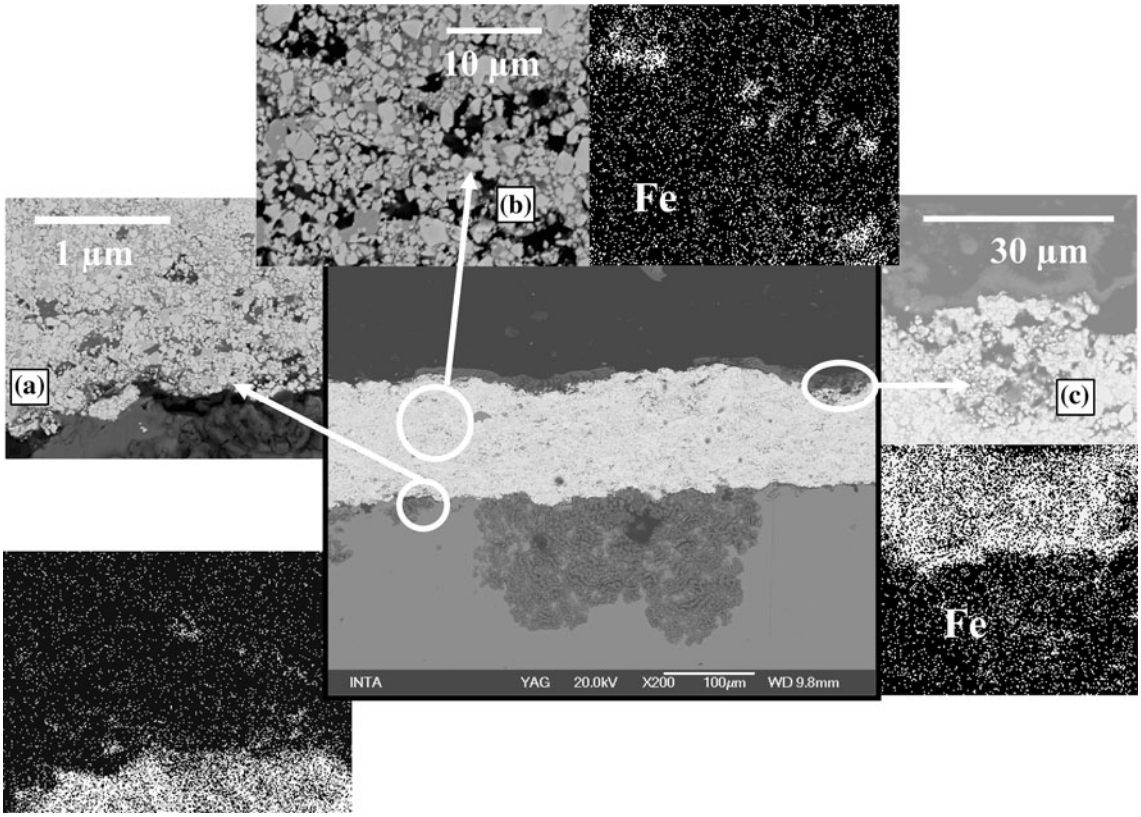

Fig. 13 Cross section of corroded WCCoCr (B′) including Fe EDS mapping of typical areas exhibiting substrate corrosion products: (a) under, (b) within, and (c) over the coating

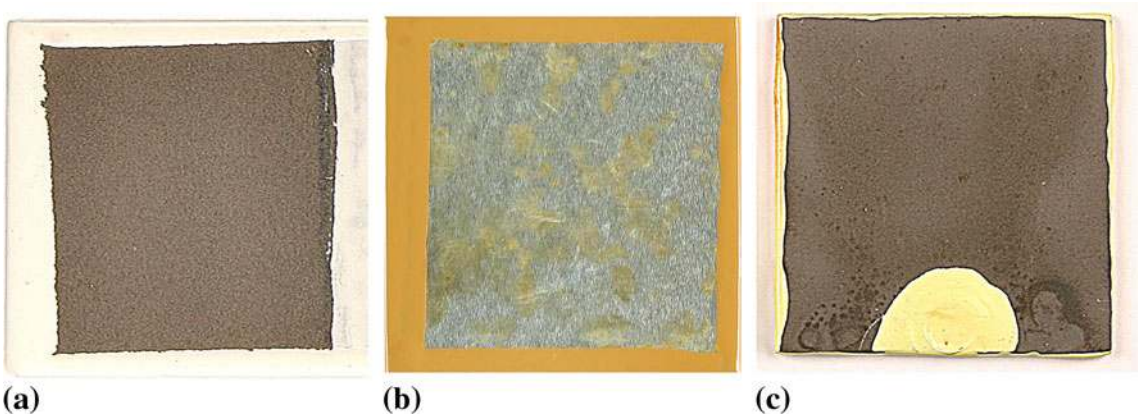

Fig. 14 Representative immersion test results after 168 h in a 33 vol.% propylene glycol solution in water (antifreeze): (a) WCCoCr (A), (b) hard Cr (batch 2), and (c) WCCoCr (B′)

A and B did not show evidence of discoloration or corrosion as shown in Fig. 14(a) where a representative coating is shown after immersion in a 33 vol.% propylene glycol solution in water (antifreeze). On the other hand, the hard Cr specimens from batch 2, as well as coating B′ did show some discoloration only when in contact with the 33 vol.% of propylene glycol in water (Fig. 14b and c, respectively), although it was considered that they both passed the test with a 0 rating, as there was no evidence of corrosion.

3.7 Wear Test

The friction coefficients as a function of sliding distance are presented in Fig. 15, whereas the average values as well as the wear rate of the four studied coatings are

shown in Table 13. All of the WCCoCr coatings exhibit an average friction coefficient of approximately 0.5 with slight variations as a function of distance but in all cases, always lower than that observed for the hard Cr coating. The coating wear coefficient was determined by measuring the wear scar with a high precision profilometer. No wear could be detected for the WCCoCr coatings, whereas the wear coefficient for the hard Cr was 2.27×10^{-4} mm^3/Nm. This is clearly illustrated in Fig. 16, where the cross sections of representative investigated samples are shown. No material loss could be observed in any of the WCCoCr coatings, whereas a significant scar is present in the hard Cr-coated specimen. Given the higher hardness of the WCCoCr coatings, these results were not unexpected. Nascimento et al. (Ref 36) and Cioffi and coworkers (Ref 11) as well as Koon et al. (Ref 25) also observed better abrasive wear resistance of WCCo and WCCoCr when compared to hard Cr coatings.

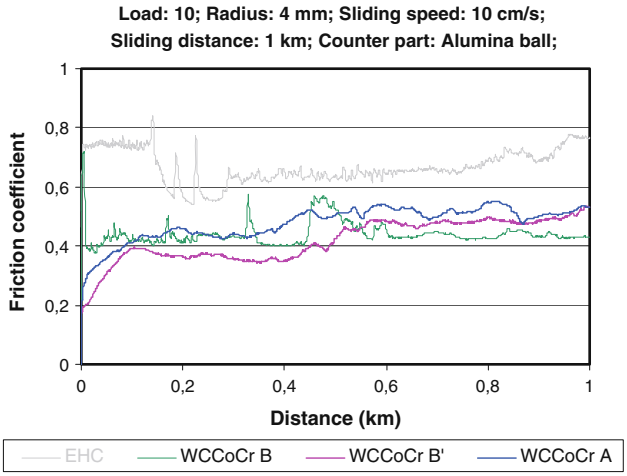

Fig. 15 Friction coefficient of the tested coatings

3.8 Fatigue Test

The S-N curves for the axial fatigue tests for 4340- as well as hard Cr- and WCCoCr-coated specimens are represented in Fig. 17. Only coating B was fatigue tested as coating B′ did not pass the salt fog corrosion test.

The hard chromium electroplating significantly decreases the fatigue resistance. It is well known that the

Table 13 Pin-on-disk test results

Sample		Friction coefficient	Wear rate, mm^3/Nm	
Name	R_a, µm	µ Average	Coating	Ball
EHC	0.0771	0.6914	227E−6	2.278E−4
A	0.1924	0.4693	ND	ND
B	0.0443	0.5164	ND	8.12E−10
B′	0.1679	0.3915	ND	ND

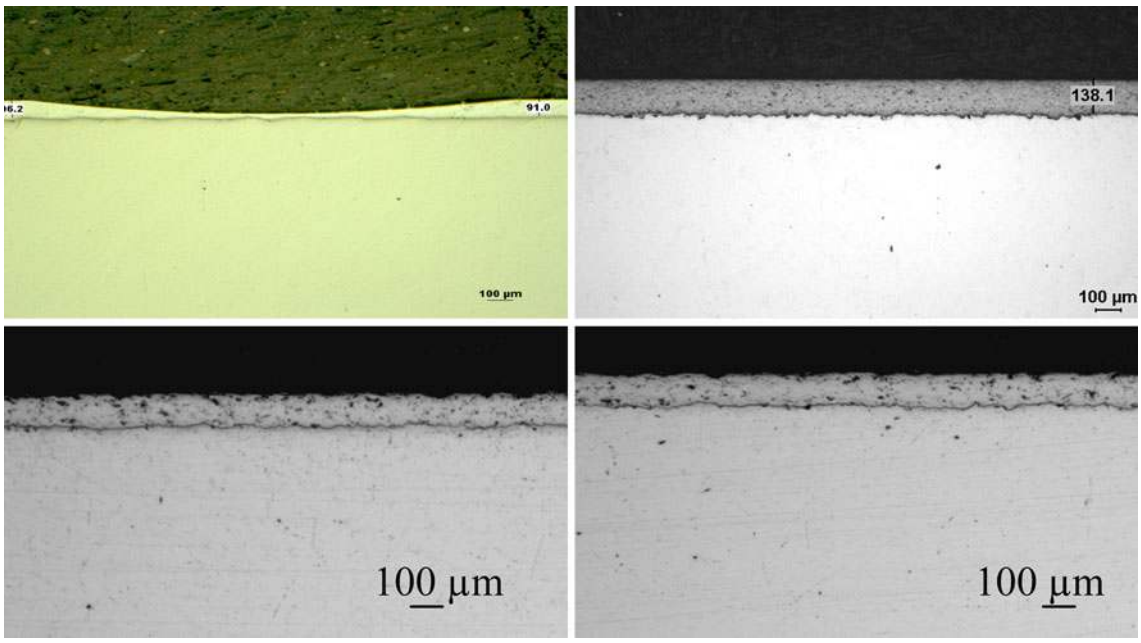

Fig. 16 Cross sections of wear tracks of (a) hard Cr, (b) WCCoCr (A), (c) WCCoCr (B), and (d) WCCoCr (B′)

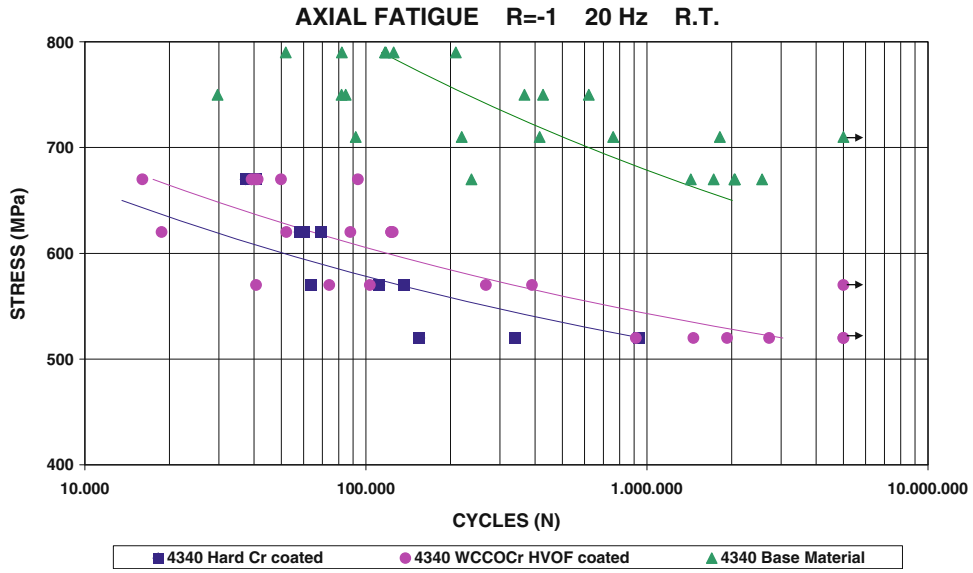

Fig. 17 Fatigue tests

hard Cr-plating process induces a tensile residual stress in the substrate, and the coating contains a high density of microcracks, which allows the crack initiation process to start at the periphery of the specimens; thus, the rate of the fatigue process increases, and the fatigue strength decreases (Ref 30, 42). The Cr-plated components are usually shot peened to improve the fatigue strength, but never to the level of the uncoated shot peened material. In the present studies, none of the tested specimens was shot peened before coating and testing.

Compared with hard Cr, the results obtained for the specimens coated with WCCoCr (B) applied by HVOF show a lower decrease in fatigue strength with respect to uncoated AISI4340. The decrease in fatigue strength relative to the uncoated substrate may be due to coating irregularities and high surface roughness ($R_a = 4.30$ μm) as these features are possible causes for cracks or nucleation/initiation sites. On the other hand, the observed better behavior when compared with the hard Cr-plated results may be explained on the basis of compressive residual stresses induced by the HVOF process on the substrate, which is beneficial for the fatigue resistance. It is important to emphasize the better fatigue strength of the WCCoCr compared with hard Cr even in spite of the higher surface roughness of the WCCoCr coatings (Ref 25). Others have shown that by shot peening before coating and testing, the fatigue strength of WCCoCr steels is significantly increased to the level of the uncoated material (Ref 11).

4. Conclusions

WCCoCr coatings were deposited by HVOF thermal spray to be used as candidates to replace electrolytic hard Cr coatings currently employed on landing gear actuators. Powders with different WC particle size and shape as well as flame energies were employed and studied, and the resulting coatings exhibited very low porosity as measured by image analysis and higher hardness than electrolytic hard Cr coating. The WC particle size differences did not appear to significantly affect the coatings microstructure and microhardness, but the spraying efficiency obtained when using the smaller particle size powder was significantly higher. This represents important savings as powder price constitute an important share of the total coating deposition cost and therefore significantly affects the overall economy of the process. Decreasing the flame energy to reduce component overheating resulted in substantial differences in microstructure and phase composition, and also caused a reduction in microhardness.

There were no significant differences in behavior in adhesion or in any of the wear and corrosion tests for the two coatings deposited with a high-energy flame. In these tests, the two coatings exhibited equal or better behavior than the hard Cr-electroplated reference. In particular, the salt fog corrosion and wear resistances of the WCCoCr exceeded by far those of the hard Cr reference.

Decreasing the flame energy to reduce component overheating resulted in similar wear and liquid immersion corrosion behavior than the other studied coatings, but a significant loss of atmospheric corrosion resistance was observed. This difference is likely due to substantial variations in microstructure and phase composition, but in any case, the low-energy flame coating is significantly better than the hard Cr reference coating.

The effect of the nano-structured WCCoCr coating applied by HVOF was to decrease the axial fatigue strength of AISI 4340 steel. However, this decrease was lower than that observed for hard Cr-electroplated specimens.

HVOF WCCoCr coatings can be used as alternative to hard Cr-electroplated coating in landing gear actuators. The nano-structured coatings can be produced with a

higher spraying efficiency representing cost savings Despite exhibiting lower corrosion resistance than the high-energy flame coatings, the low-energy flame WCCoCr still exceeds the performance of the hard Cr reference and can therefore offer further reduction of processing costs and complexity as component cooling will not be required.

Acknowledgments

This study has been partly financed by the Spanish Ministry of Education and Science under project CIT-370200-2005-18 ''Environmentally Compliant Coatings as Alternatives for Hard-Cr, Cd and Ni'' (RAMPE). The authors are grateful to the partners of RAMPE: AERNNOVA, CESA, GUTMAR, ITP, SENER, and TEKNIKER for their support, especially to CESA for providing the substrate material employed in the project. The contribution of SULZER-WOKA is also acknowledged as thermal spray powder supplier. The authors express their thanks to the personnel at the Metallic Materials Area of INTA, for their valuable contribution, in particular to Dr. A. Sánchez Pascual, the former head of that Area, and F. Longo its present head, for their support.

References

1. K.R. Newby, Industrial (Hard) Chromium Plating, *Surface Engineering*, ASM Handbook, ASM International, Materials Park, OH, 1994, p 177-191
2. H.J. Gibb, P.S.J. Lees, P.F. Pinsky, and B.C. Rooney, Lung Cancer Among Workers in Chromium Chemical Production, *Am. J. Ind. Med.*, 2000, **38**, p 15-126
3. Occupational Exposure to Hexavalent Chromium, Final Rule, Rules and Regulations, OSHA, *Federal Register*, 71, 2006, p 10999-10385
4. K.O. Legg, Overview of Chromium and Cadmium Alternative Technologies, *Surface Modification Technologies XV*, T.S. Sudarshan and M. Jeandin, Ed., ASM International, Materials Park, OH, 2002, p 1-10
5. P.M. Natishan, S.H. Lawrence, R.L. Foster, J. Lewis, and B.D. Sartwell, Corrosion Behavior of HVOF Thermal Spray Coatings Compared to Electrodeposited Hard Chromium, *Surf. Coat. Technol.*, 2000, **130**, p 218-223
6. J.A. Picas, A. Forn, and G. Matthäus, HVOF Coatings as an Alternative to Hard Chromium for Pistons and Valves, *Wear*, 2006, **261**, p 477-484
7. C. Reigner, A. Sturgeon, D. Lee, and D. De Wet, HVOF Sprayed WC-Co-Cr as a Generic Coating Type for Replacement of Hard Chromium Plating, *Proceedings of the International Thermal Spray Conference*, May 2002 (Dusseldorf, Germany), 2002, p 12-16
8. D. Dudzinski, P. Au, J.G. Legoux, and S. Simard, Salt Fog Corrosion Resistance of HVOF WC-10C0-4Cr Coated and Electrolytic Hard Chromium Plated AerMet 100 and 300M Steel Alloys, *Proceedings of the International Thermal Spray Conference*, May 2002 (Dusseldorf, Germany), 2002, p 686-692
9. D. Lee, E. Eybel, and R. Evans, Development and Implementation of HVOF WC/Co/Cr Coating as Alternative to Electrolytic Hard Chrome Plate in Landing Gear Applications Using Natural Gas as Fuel, *Thermal Spray 2003*, May 2003 (Orlando, FL), 2003, p 371-376
10. B. Sartwell, K.O. Legg, J. Schell, J. Sauer, P. Natishan, D. Dull, J. Falkowski, P. Bretz, J. Deveraux, C. Edwards, and D. Parker, Validation of HVOF WC/Co Thermal Spray Coatings as a Replacement for Hard Chrome Plating on Aircraft Landing Gear, *Naval Research Laboratory*, Report No. NRL/MR/6170-04-8762, 2004, http://www.estcp.org/viewfile.cfm?doc=PP-9608-FR-01.pdf
11. H. Voorwald, R. Souza, W. Pigatin, and M. Cioffi, Evaluation of WC-17Co and WC-10Co-4Cr Thermal Spray Coatings by HVOF on the Fatigue and Corrosion Strength of AISI, 4340 Steel, *Surf. Coat. Technol.*, 2005, **190**, p 155-164
12. K. Jia and T.E. Fisher, Abrasion Resistance of Nanostructured and Conventional Cemented Carbides, *Wear*, 1996, **200**, p 206-214
13. K. Jia and T.E. Fisher, Sliding Wear of Conventional and Nanostructured Cemented Carbides, *Wear*, 1997, **203-204**, p 310-318
14. T.Y. Cho, J.H. Yoon, K.S. Kim, K.O. Song, Y.K. Joo, W. Fang, S.H. Zhang, S.J. Youn, H.G. Chun, and S.Y. Hwang, A Study on HVOF Coatings of Micron and Nano WC-Co Powders, *Surf. Coat. Technol.*, 2008, **202**, p 5556-5559
15. J.M. Guilemany, S. Dosta, and J.R. Miguel, The Enhancement on the Properties of WC-Co HVOF Coatings Through the Use of Nanostructured and Microstructured Feedstock Powders, *Surf. Coat. Technol.*, 2006, **201**, p 1180-1190
16. J.P. Sauer and P. Sahoo, HVOF Process Control Using Almen and Temperature Measurement, www.imrlouisville.com/cms/repository/
17. L.M. Berger, W. Hermel, P. Vuoristo, T. Mäntylä, W. Lengauer, and P. Ettmayer, Structure Properties and Potentials of WC-Co, Cr_3C_2-NiCr and TiC-Ni-Based Hardmetal like Coatings, *Thermal Spray: Practical Solutions for Engineering Problems*, ASM Thermal Spray Society, Cincinnati, OH, 1996, p 89-96
18. R.A. Young, *The Rietveld Method*, Oxford Science Publications, Oxford, 1993
19. L.M. Berger, P. Ettmayer, P. Vuoristo, T. Mäntyla, and W. Kunert, Microstructure and Properties of WC-10%Co-4% Cr Spray Powders and Coatings: Part 1. Powder Characterization, *J. Therm. Spray Technol.*, 2000, **10**, p 311-325
20. C. Verdon, A. Karimi, and J.-L. Martin, A Study of High Velocity Oxy-Furl Thermally Sprayed Tungsten Carbide Based Coatings. Part 1: Microstructures, *Mater. Sci. Eng. A*, 1998, **246**, p 11-24
21. S. Bouaricha and J.G. Legoux, Controlling the Degradation Phenomena During HVOF Spraying of WC-10Co-4Cr Cermet, *Proceedings of the International Thermal Spray Conference*, ASM Thermal Spray Society, Essen, Germany, 2002, p 295-299
22. M.H. Li, D. Shiand, and P.D. Christofides, Modeling and Control of HVOF Thermal Spray Processing of WC-Co Coatings, *Powder Technol.*, 2005, **156**, p 177-194
23. C.J. Li, G.C. Ji, Y.Y. Wang, and K. Sonoya, Dominant Effect of Carbide Rebounding on the Carbon Loss During High Velocity Oxy-Fuel Spraying of Cr_3C_2-NiCr, *Thin Solid Films*, 2002, **419**, p 137-143
24. C.J. Li, A. Ohmori, and Y. Harada, Formation of an Amorphous Phase in Thermally Sprayed WC-Co, *J. Therm. Spray Technol.*, 1996, **5**, p 69-73
25. A.P. Koon, T.D. Hee, M. Taylor, M. Weston, and J. Yip, Hard Chrome Replacement by HVOF Sprayed Coatings, *SIM Tech Technical Report* (PT/99/002/ST), Singapore Institute of Manufacturing Technology, 1999, p 1-8
26. P. Chivavibul, M. Watanabe, S. Kuroda, and K. Shinoda, Effects of Carbide Size and Co Content on the Microstructural and Mechanical Properties of hVOF-Sprayed WC-Co Coatings, *Surf. Coat. Technol.*, 2007, **202**, p 509-521
27. J. Berget, T. Rogne, and E. Bardal, Erosion-Corrosion Properties of Different WC-Co-Cr Coatings Deposited by the HVOF Process-Influence of Metallic Matrix Composition and Spray Powder Distribution, *Surf. Coat. Technol.*, 2007, **201**, p 7619-7625
28. D.A. Stewart, P.H. Shipway, and D.G. McCartney, Microstructural Evolution in Thermally Sprayed WC-Co Coatings: Comparison Between Nanocomposite and Conventional Starting Powders, *Acta Mater.*, 2000, **48**, p 1593-1604
29. J.G. Legoux and S. Bouaricha, Evaluation of Starting Material and Process Parameters for HVOF WC-10Co-4Dr Coatings, *Proceedings of the International Thermal Spray Conference*, ASM Thermal Spray Society, Essen, Germany, 2002, p 289-294

30. A. Ibrahim and C.C. Berndt, Fatigue and Deformation of HVOF Sprayed WC-Co Coatings and Hard Chrome Plating, *Mater. Sci. Eng. A*, 2007, **456**, p 114-119
31. A.A. Tipton, The Effect of HVOF Sprayed Coatings on the Elevated Temperature High Cycle Fatigue Behaviour of Martensitic Stainless Steel, *Proceedings of the 6th National Thermal Spray Conference on Advances in Thermal Spray Science and Technology* (Houston), ASM International, TX, 1995, p 463-468
32. L. Zhao, M. Maurer, F. Fischer, R. Dicks, and E. Lugscheider, Influence of Spray Parameters on the Particle In-Flight Properties and the Properties of HVOF Coating of WC-CoCr, *Wear*, 2004, **257**, p 41-46
33. H. Engqvist, S. Ederyd, N. Axen, and S. Hogmark, Grooving Wear of Single-Crystal Tungsten Carbide, *Wear*, 1999, **230**, p 165-174
34. G.S. Pisarenki, V.A. Borisenko, and Y.A. Kashtalyan, Effect of Temperature on the Hardness and Modulus of Elasticity of Tungsten and Molybdenum in the Temperature Range of 20 to 2700°C, *Sov. Powder Metall. Met. Ceram.*, 1962, **5**, p 371-372 ((translated from Russian))
35. A.R. Jones, Microcracks in Hard Chromium Electrodeposits, *Plat. Surf. Finish.,* 1989, p 62-66
36. M. Nascimento, R. Souza, I. Miguel, W. Pigatin, and H. Voorwald, Effects of Tungsten Carbide Thermal Spray Coating by HP/HVOF and Hard Chromium Electroplating on AISI, 4340 High Strength Steel, *Surf. Coat. Technol.*, 2001, **138**, p 113-124
37. B.E. Bodger, R.T.R. Megram, and D.A. Sommerville, The Evaluation of Tungsten Carbide Thermal Spray Coatings as Replacements for Electrodeposited Chrome Plating on Aircraft Landing Gear, *Plat. Surf. Finish.*, 1997, p 28-31
38. A.A. Ashary and R.C. Tucker, Corrosion Characteristic of Selected Thermal Spray Coatings, *Corrosion* 93, 1993, Paper No. 24
39. A.A. Ashary and R.C. Tucker, Electrochemical and Long-Term Corrosion Studies of Several Alloys in Bare Condition and Plasma Sprayed with Cr_2O_3, *Surf. Coat. Technol.*, 1989, **43-44**, p 567-576
40. S. Simard, Performance of HVOF-Sprayed Carbide Coatings in Aqueous Corrosive Environments, *Proceedings of the 1st International Thermal Spray Conference*, May 2000 (Montreal, Canada), 2000, p 982-990
41. G. Bolelli, L. Lusvarghi, and R. Giovanardi, A Comparison Between the Corrosion Resistances of Some HVOF-Sprayed Metal Alloy Coatings, *Surf. Coat. Technol.*, 2008, **202**, p 4793-4809
42. R. Souza, H. Voorwald, and M. Cioffi, Fatigue Strength of HVOF Sprayed Cr_3C_2-25NiCr and WC-10Ni on AISI, 4340 Steel, *Surf. Coat. Technol.*, 2008, **203**, p 191-198